Evidence for a major structural change in *Escherichia coli* chorismate synthase induced by flavin and substrate binding

Peter MACHEROUX*†[1,2], Ernst SCHÖNBRUNN*, Dmitri I. SVERGUN‡§, Vladimir V. VOLKOV§, Michel H. J. KOCH‡, Stephen BORNEMANN† and Roger N. F. THORNELEY†[2]

*ETH-Zürich, Institute of Plant Sciences, Universitätstr. 2, CH-8092 Zürich, Switzerland, †Nitrogen Fixation Laboratory, John Innes Centre, Norwich Research Park, Colney, Norwich NR4 7UH, U.K., ‡EMBL, Hamburg Outstation, Notkestrasse 85, D-22603, Hamburg, Germany, and §Institute of Crystallography, Russian Academy of Sciences, Leninsky pr. 59, 117333 Moscow, Russia

Chorismate synthase (EC 4.6.1.4) catalyses the conversion of 5-enolpyruvylshikimate 3-phosphate (EPSP) into chorismate, and requires reduced FMN as a cofactor. The enzyme can bind first oxidized FMN and then EPSP to form a stable ternary complex which does not undergo turnover. This complex can be considered to be a model of the ternary complex between enzyme, EPSP and reduced FMN immediately before catalysis commences. It is shown that the binding of oxidized FMN and EPSP to chorismate synthase affects the properties and structure of the protein. Changes in small-angle X-ray scattering data, decreased susceptibility to tryptic digestion and altered Fourier-transform (FT)-IR spectra provide the first strong evidence for major structural changes in the protein. The tetrameric enzyme undergoes correlated screw movements leading to a more overall compact shape, with no change in oligomerization state. The changes in the FT-IR spectrum appear to reflect changes in the environment of the secondary-structural elements rather than alterations in their distribution, because the far-UV CD spectrum changes very little. Changes in the mobility of the protein during non-denaturing PAGE indicate that the ternary complex may exhibit less conformational flexibility than the apoprotein. Increased enzyme solubility and decreased tryptophan fluorescence are discussed in the light of the observed structural changes. The secondary structure of the enzyme was investigated using far-UV CD spectroscopy, and the tertiary structure was predicted to be an α–β-barrel using discrete state-space modelling.

INTRODUCTION

Chorismate synthase (EC 4.6.1.4), the seventh enzyme of the shikimate pathway, catalyses the conversion of 5-enolpyruvylshikimate 3-phosphate (EPSP) into chorismate (Scheme 1). Being present in bacteria and fungi, but not in mammals, this enzyme is an attractive target for new anti-microbial agents. This promise has recently been realized by the discovery of a functional shikimate pathway in apicomplexan parasites, including malaria, that can be inhibited with chemotherapeutic effect [1]. The reaction comprises an *anti*-1,4-elimination of the 3-phosphate group and the C(6*proR*) hydrogen [2–4]. This reaction is the only known example of such a transformation in biological systems and makes chorismate synthase a unique enzyme. Although this reaction does not involve an overall change in redox states, the reaction has an absolute requirement for reduced FMN [5–7]. The radical mechanism shown in Scheme 1, whereby the flavin transiently donates an electron to EPSP to facilitate the loss of phosphate, has recently been proposed to account for this absolute requirement [8]. Spectroscopic studies with FMN and its analogues have shown that the enzyme binds reduced $FMNH^-$ in its anionic form and that it experiences a more apolar environment on the binding of EPSP, resulting in it being protonated and having a lower redox potential [9–11]. Kinetic studies have shown that this protonation precedes any bond-breaking steps associated with the substrate [12]. FMN in its oxidized form binds to chorismate synthase with a K_d of approx. 30 μM; in the presence of the substrate EPSP, binding becomes three orders of magnitude tighter, to give a K_d of approx. 20 nM [9]. The substrate-induced enhanced binding of oxidized FMN leads to UV/visible spectral and fluorescent changes associated with the flavin, which indicate that the flavin-binding pocket becomes more apolar in the presence of EPSP. This tightly bound ternary complex does not undergo turnover because activity requires the flavin to be reduced. Thus the stable ternary complex between enzyme, EPSP and oxidized FMN can be considered to be a good structural model of the corresponding active ternary complex formed with reduced FMN immediately before catalysis commences.

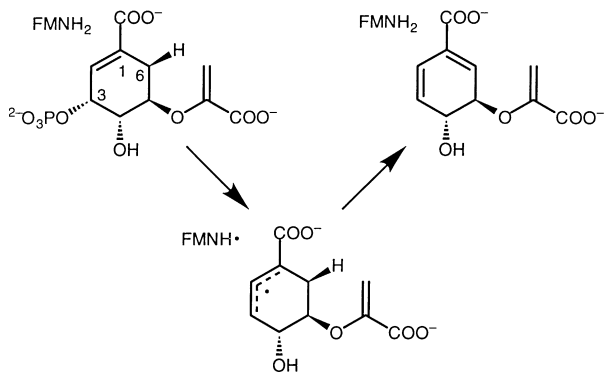

Scheme 1 Conversion of EPSP into chorismate by chorismate synthase

While these effects on the flavin have been reported recently [9,11], any associated changes in the properties and structure of the protein have not previously been addressed. In the present paper it is shown that binding of EPSP and oxidized FMN to

Abbreviations used: EPSP, 5-enolpyruvylshikimate 3-phosphate; FT-IR, Fourier-transform IR.

[1] Present address: ETH-Zürich, Institute of Plant Sciences, Universitätstr. 2, CH-8092 Zürich, Switzerland.
[2] To whom correspondence should be addressed (e-mail roger.thorneley@bbsrc.ac.uk).

chorismate synthase affects the properties and structure of the protein. Changes in small-angle X-ray scattering data, decreased susceptibility to proteolytic digestion and altered Fourier-transform (FT)-IR spectra provide the first strong evidence for major structural changes in the protein. Increased mobility of the protein in non-denaturing PAGE, increased enzyme solubility, decreased tryptophan fluorescence, little change in far-UV CD spectra and secondary structure evaluations and predictions are discussed in the light of the observed structural changes.

EXPERIMENTAL

Materials

Chorismate synthase was purified from an overproducing strain of *Escherichia coli* (AB2849/pGM605), as described previously [13]. From 20 g of cell paste, 125 mg of enzyme was obtained with a purity of $> 95\,\%$ as judged by SDS/PAGE. The enzyme was stored in bead form in liquid nitrogen. FMN (approx. 95 %) was obtained from Sigma Chemical Co. (Poole, Dorset, U.K.), and the potassium salt of EPSP was prepared as described by Knowles et al. [14].

Fluorescence emission measurements

Fluorescence emission spectra were obtained with a Kontron SFM25 spectrofluorimeter at 25 °C. The excitation wavelength used for tryptophan fluorescence was 280 nm. Experiments were carried out in 50 mM Mops/10 % glycerol, pH 7.5.

Stopped-flow spectrofluorimetry

The rate of fluorescence quenching was determined using a Hi-Tech Scientific SF-61-DX2 stopped-flow spectrofluorimeter (Salisbury, U.K.). Fluorescence excitation was at 440 nm using a Xenon lamp, and fluorescence emission was detected above 455 nm with the aid of a cut-off filter. Experiments were carried out in 50 mM Mops/10 % glycerol, pH 7.5, at 25 °C.

CD spectroscopy

CD spectra were recorded with a Jasco J-710 spectropolarimeter at 20 °C with a 2 mm path-length cuvette. A total of 25 spectra were accumulated for each sample and corrected by subtracting contributions from the buffer.

PAGE

Non-denaturing PAGE was performed using the Pharmacia PhastSystem with an 8–25 % gel run at pH 8.8 for 240 AVh over a period of 45 min at 15 °C. The chorismate synthase apoprotein is predicted to have a pI of approx. 6.1 and to have a net charge of between -7 and -10 at pH 8.8. Gels were stained with Coomassie Blue. Oxidized FMN and substrate were added in 5-fold molar excess to samples of enzyme (12.8 μM, in 50 mM Mops buffer, pH 7.5) as indicated in Figure 4, 20 min before starting the electrophoresis. Jack-bean urease (545 and 272 kDa) and BSA (132 and 66 kDa) were used as protein standards. Denaturing SDS/PAGE was performed as described by Laemmli [15]. Protein standards (Sigma; MW-SDS-70L kit) were: BSA, 66 kDa; egg albumin, 45 kDa; rabbit muscle glyceraldehyde-3-phosphate dehydrogenase, 36 kDa; bovine erythrocyte carbonic anhydrase, 29 kDa; bovine pancreas trypsinogen, 24 kDa; soybean trypsin inhibitor, 20.1 kDa; bovine milk α-lactalbumin, 14.1 kDa.

FT-IR spectroscopy

Spectra were recorded with a Perkin–Elmer IR spectrometer (system 2000) equipped with a sample shuttle. The instrument was purged with a continuous flow of dry nitrogen gas both before and during data acquisition. Spectra were calculated from 80 scans obtained at 4 cm^{-1} resolution over a 20 min acquisition period. Compensation for water vapour was achieved with one scan of the reference cuvette before and after four scans of the sample cuvette. Sample spectra were then corrected with buffer spectra recorded under identical conditions on the same day. Protein concentration was 0.5 mM in 10 mM sodium phosphate buffer, pH 7.5. IR spectra were recorded using calcium fluoride windows using 15 μm spacers at 25 °C.

Small-angle X-ray scattering experiments and data treatment

The synchrotron radiation X-ray scattering data were collected following standard procedures using the European Molecular Biology Laboratory X33 camera [16–18] on the storage ring DORIS III of the Deutsches Elektronen Synchrotron (DESY) with multiwire proportional chambers and delay line readout [19]. At a sample-detector distance of 2 m and a wavelength λ of 0.15 nm, the range of momentum transfer $0.23 < s < 4.5$ nm^{-1} was covered ($s = 4\pi\sin\Theta/\lambda$, where 2Θ is the scattering angle). Samples with concentrations of 7–12 mg·3 ml^{-1} were used. All data processing procedures (normalization, buffer subtraction, etc.) involved statistical errors propagation using the program SAPOKO (D.I Svergun and M. H. J. Koch, unpublished work).

The maximum diameters of particles were estimated from the scattering curves using the orthogonal expansion program ORTOGNOM [20]. The values of the forward scattering (which is proportional to the molecular mass of the solute) and the radii of gyration were evaluated using the indirect transform program GNOM [21,22].

Shape determination from small-angle X-ray scattering data

The *ab initio* shape determination from experimental solution scattering curves followed the method of Svergun and Stuhrmann [23] and Svergun et al. [24]. The envelope of the particle is represented by an angular border function $F(\omega)$, where $\omega = (\Theta, \phi)$ are spherical co-ordinates, which is parameterized as:

$$F(\omega) = \sum_{I=0}^{L} \sum_{m=-1}^{I} f_{Im} Y_{Im}(\omega) \tag{1}$$

where f_{lm} are complex numbers and $Y_{lm}(\omega)$ are spherical harmonics. The resolution of this representation, defined by the truncation parameter L, is equal to $\delta r = \pi R_0/(L+1)$, where R_0 is the radius of the equivalent sphere. The algorithms to rapidly calculate the scattering intensity $I(s)$ from such a model, taking into account the particle/solvent interface, are described by Svergun [25] and Svergun and Stuhrmann [23]. The shape determination was performed using terms up to $L = 6$ and assuming a 222-point symmetry of the tetrameric molecule, which yields 13 free parameters f_{lm} in expansion (see eqn. 1). These parameters were determined by a non-linear optimization procedure by minimizing the R-factor between the calculated and the experimental curves:

$$R^2 = \frac{\sum_{j=1}^{N} \{[I(s_j) - I_{exp}(s_j)]/\sigma(s_j)\}^2}{\sum_{j=1}^{N} [I_{exp}(s_j)/\sigma(s_j)]^2} \tag{2}$$

where N is the number of experimental points, and $I_{exp}(s)$ and $\sigma(s)$ are the experimental intensity and its S.D. respectively. A sphere was used as an initial approximation; additional penalties to keep the particle surface smooth and the envelope function positive definite are described by Svergun et al. [24]. A constant term was subtracted from each scattering curve prior to the shape determination to remove the unwanted scattering due to the atomicity of the structure and to ensure that the intensity decay was proportional to s^{-4} at higher angles, in accordance with Porod's law for homogeneous bodies [26].

Global secondary structure evaluation based on protein CD spectra

CD spectra were recorded in the range 178–260 nm, and the measured ellipticity was converted into molar CD using the following equation:

$$\text{molar CD} = (113 \times 30 \times 10^{-6})/(c \times l)$$

where 113 is the average molecular mass (Da) of an amino acid, 30×10^{-6} is the factor used to convert observed ellipticity into ΔA, c is the concentration of the protein in mg·ml^{-1} and l is the path length of the cuvette in cm. The contribution of α-helix, β-sheets, turns and loops and undefined structures was determined using the program SELCON [27].

Secondary and tertiary structure predictions

The secondary structure of *E. coli* chorismate synthase was predicted using type-1 discrete state-space modelling [28,29]. The 361-amino-acid long *E. coli* chorismate synthase sequence was trimmed by the N-terminal methionine and the last 10 amino acids of the C-terminus, and numbered from 1 to 350 accordingly.

Determination of strictly conserved amino acids in chorismate synthases

Strictly conserved amino acids were identified by aligning the following 18 chorismate synthase sequences (accession numbers given in parentheses): *Archaeoglobus fulgidus* (AF0670) [30], *Bacillus subtilis* (P31104), *Corydalis sempervirens* (precursor; X60544), *E. coli* (M27714), *Haemophilus influenzae* (P43875), *Helicobacter pylori* (HP0663) [31], *Lycopersicon esculentum* (precursor 1; Z21796), *Lycopersicon esculentum* (precursor 2; Z21791), *Methanococcus jannaschii* (MJ1175) [32], *Mycobacterium tuberculosis* (P95013), *Neurospora crassa* (U25818), *Plasmodium falciparum* (AF008549), *Saccharomyces cerevisiae* (X60190), *Salmonella typhimurium* (M27715), *Staphylococcus aureus* (U31979), *Synechocystis* sp., strain PCC6803 (P23353), *Toxoplasma gondii* (U93689) and *Vibrio anguillarum* (P39198).

RESULTS

Effects of EPSP and oxidized FMN on the solubility of chorismate synthase

The solubility of apo-chorismate synthase is approx. 30 μM in 10 mM potassium phosphate buffer, pH 7.5, at 4 °C. At higher concentrations the protein forms an amorphous white precipitate. The solubility of the enzyme is increased to a small extent with higher phosphate concentrations, the addition of glycerol and an increase in temperature. By contrast, EPSP increases the solubility of the enzyme considerably. The addition of equimolar amounts of EPSP re-solubilizes the precipitated enzyme completely without any detectable loss of the original activity. Protein concentrations of up to approx. 2 mM could be obtained in the presence of EPSP. Oxidized FMN alone does not affect protein solubility.

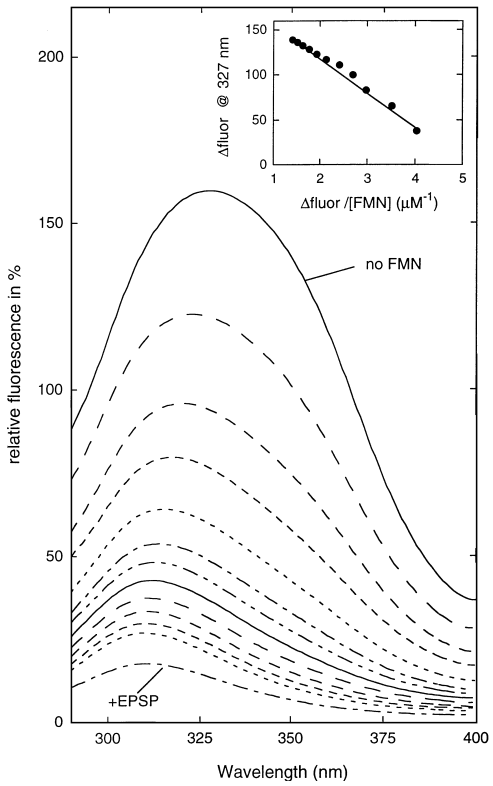

Figure 1 Chorismate synthase tryptophan fluorescence quenching by oxidized FMN and EPSP

Chorismate synthase (16 μM) in 50 mM Mops buffer, pH 7.5, containing 10% glycerol at 25 °C was titrated with FMN stock solution (1.88 mM). The spectra were recorded at the following final FMN concentrations (from top to bottom): 0, 9.4, 18.6, 27.8, 36.9, 45.9, 54.8, 63.6, 72.3, 81, 89.5 and 98 μM. The final spectrum was recorded after the addition of EPSP (62 μM, bottom spectrum), and was considered to represent maximal fluorescence quenching. The excitation wavelength was 280 nm. Inset: changes in fluorescence emission at 327 nm (Δfluor), taken from the titration data, are plotted and fitted to the equation $\Delta\text{fluor} = \Delta\text{fluor(max)} - K_d \times \Delta\text{fluor}/[\text{FMN}]$ using linear regression to give the solid line. A K_d of 37 μM for oxidized FMN was obtained from the slope.

Tryptophan fluorescence quenching on binding of oxidized FMN and EPSP

E. coli chorismate synthase contains two tryptophans, one at the C-terminus (Trp-361; numbering with respect to full *E. coli* sequence, including N-terminal methionine) and the other in the central part of the amino acid sequence (Trp-170). Titration of chorismate synthase with oxidized FMN caused a decrease in the tryptophan fluorescence of approx. 90% (Figure 1). From the graphical data analysis shown in the inset to Figure 1, a dissociation constant of 37 μM for oxidized FMN was determined. This value is in good agreement with a recently reported dissociation constant of 30 μM [9]. Upon addition of one equivalent of EPSP with respect to chorismate synthase and oxidized FMN (16 μM each), the tryptophan fluorescence was quenched to the same degree as in the presence of a large excess of FMN. This is a consequence of the much lower dissociation constant of approx. 20 nM for oxidized FMN in the presence of EPSP [9]. Note that the absence of reduced FMN in these experiments precludes any turnover by the enzyme. Similarly, in

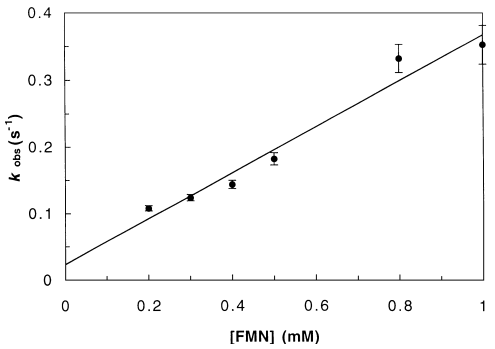

Figure 2 Kinetics of binding of oxidized FMN to chorismate synthase

Oxidized FMN (0.2–1.0 mM after mixing) was rapidly mixed with chorismate synthase (25 μM after mixing) in 50 mM Mops buffer, pH 7.5, using a stopped-flow spectrofluorimeter, and the rate of FMN fluorescence quenching was determined. The k_{on} and k_{off} values were determined to be 350 ± 30 $M^{-1} \cdot s^{-1}$ and 0.02 ± 0.02 s^{-1} from the slope and intercept respectively of the plot of the observed pseudo-first-order rate against FMN concentration. The value of the correlation coefficient, r^2, was 0.96, and the bars represent S.E.M. values estimated from triplicate determinations.

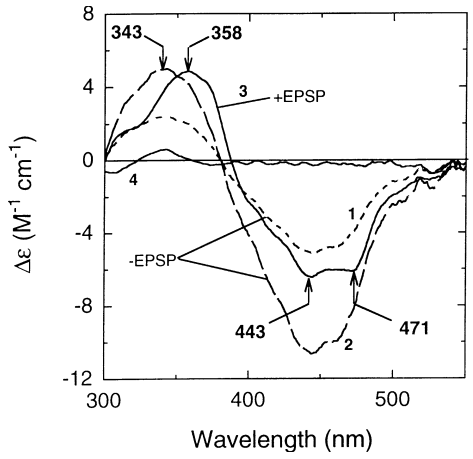

Figure 3 Changes in the UV/visible CD spectrum of enzyme-bound oxidized FMN in the presence of EPSP

The observed spectrum of oxidized FMN (66 μM) in 50 mM Mops buffer, pH 7.5, containing 10% glycerol at 20 °C in the presence of chorismate synthase (66 μM) (spectrum 1, dotted line) was corrected for the calculated concentration of enzyme-bound FMN (spectrum 2, dashed line). The spectrum changed upon addition of EPSP (67 μM) (spectrum 3, solid line). Free FMN exhibits little or no CD under these conditions (spectrum 4, solid line).

the presence of equimolar concentrations of reduced FMN alone, the tryptophan fluorescence was also quenched markedly by approx. 70%, again consistent with the much lower dissociation constant of 18 nM for reduced FMN [9].

Rapid kinetics of binding of oxidized FMN to chorismate synthase

When chorismate synthase (25 μM after mixing) was rapidly mixed with an excess of oxidized FMN (0.2–1.0 mM after mixing) in the stopped-flow apparatus, the pseudo-first-order rate of flavin fluorescence quenching showed a linear dependence on the FMN concentration (Figure 2). This experiment yielded values for k_{on} and k_{off} of 350 ± 30 $M^{-1} \cdot s^{-1}$ and 0.02 ± 0.02 s^{-1} respectively. The large errors, particularly at high FMN concentrations, are a result of the relatively small observable fluorescence change

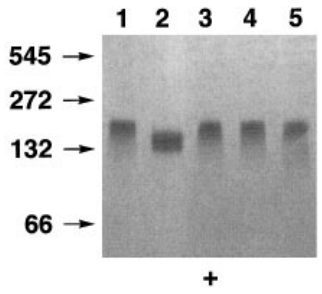

Figure 4 Increased mobility of chorismate synthase during non-denaturing PAGE when pre-incubated with both EPSP and oxidized FMN

Chorismate synthase (13 μM) was incubated with or without a 5-fold molar excess of EPSP and oxidized FMN for 20 min in 50 mM Mops buffer, pH 7.5, before electrophoresis. Lanes: 1, chorismate synthase; 2, chorismate synthase, FMN and EPSP; 3, chorismate synthase; 4, chorismate synthase and FMN; 5, chorismate synthase and EPSP. The positions of molecular mass standards are indicated in kDa.

compared with the total fluorescence signal. This is due to the FMN concentration being in excess of the enzyme concentration to allow for pseudo-first-order conditions. A dissociation constant of 60 μM can be calculated from the rate constants. This value is of the same order as, and therefore consistent with, that obtained from the tryptophan fluorescence quenching experiment described above (37 μM).

When chorismate synthase was pre-incubated with EPSP prior to mixing with oxidized FMN, a lower rate of fluorescence quenching was observed. Importantly, the system reached equilibrium within a few minutes in all cases. With a 5–20-fold excess of EPSP over chorismate synthase, this rate was found to be independent of the EPSP concentration. This result suggests that the K_d for EPSP is lower than that for oxidized FMN, and that there is a compulsory order of binding of oxidized FMN and then EPSP to form a ternary complex where, at high substrate concentrations, the binding of FMN is limited by the dissociation of EPSP from the enzyme. This result is consistent with previous order-of-mixing studies [33], which have shown that the catalytically competent ternary complex of chorismate synthase, reduced FMN and EPSP appears to form with the same order of binding.

Effect of EPSP on the UV/visible CD spectrum of enzyme-bound oxidized FMN

The CD spectrum of oxidized FMN in the presence of chorismate synthase has a negative peak at 445 nm and a positive one at 343 nm (Figure 3, spectrum 1). Since the K_d of oxidized FMN is 30 μM [9], only 48% of oxidized FMN would have been bound to the enzyme at the concentrations used. The spectrum was adjusted to give that expected for 100% binding (Figure 3, spectrum 2). Addition of an equimolar concentration of EPSP caused a shift of the short-wavelength maximum from 343 to 358 nm and an increase in the resolution of the peak at longer wavelength (Figure 3, spectrum 3). This spectrum required no correction, because the K_d for oxidized FMN in the presence of EPSP is 20 nM [9], resulting in stoichiometric binding at these concentrations. Free FMN exhibits no strong CD features under these conditions (Figure 3, spectrum 4).

Non-denaturing PAGE of chorismate synthase with and without pre-incubation with EPSP and oxidized FMN

Figure 4 shows a non-denaturing PAGE analysis of chorismate synthase. When applied to the gel alone, more than 90% of the

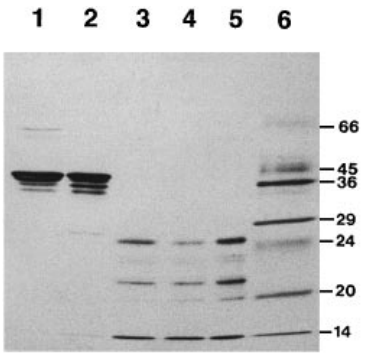

Figure 5 EPSP and oxidized FMN together protect chorismate synthase from tryptic digestion

Chorismate synthase (14.5 μg), with or without a 3.5-fold molar excess of EPSP and oxidized FMN, was incubated with trypsin (30 ng) for 1 h at 25 °C in 50 mM Mops buffer/10% glycerol, pH 7.5, and subjected to SDS/PAGE with silver staining. Lanes 1, chorismate synthase, no additions; 2, chorismate synthase, EPSP, FMN and trypsin; 3, chorismate synthase, EPSP and trypsin; 4, chorismate synthase, FMN and trypsin; 5, chorismate synthase and trypsin; 6, molecular mass standards indicated in kDa.

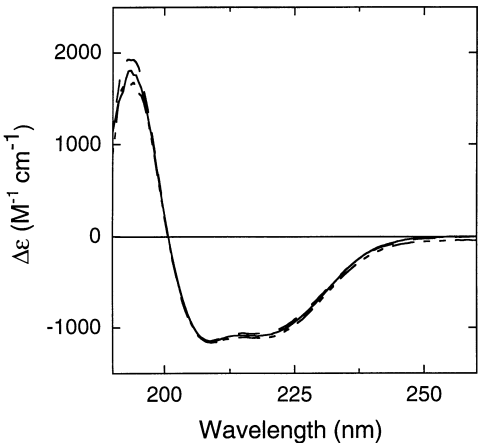

Figure 6 The far-UV CD spectrum of chorismate synthase changes very little on addition of EPSP and oxidized FMN

The CD spectrum of chorismate synthase (2 μM) in 10 mM potassium phosphate buffer, pH 7.5, at 20 °C is shown by the solid line. Spectra in the presence of EPSP only (6.2 μM) and both EPSP (6.2 μM) and FMN (2.6 μM) are shown as dotted/dashed and dashed lines respectively.

protein migrated with an apparent molecular mass of about 190 kDa. Since the molecular mass of the homotetramer of chorismate synthase is predicted to be 156 kDa from the amino acid sequence and electrospray mass spectrometry of the monomer [34], the protein appears to exhibit either a larger than expected hydrodynamic volume or a lower net negative charge than expected. Although no monomers, dimers or higher oligomers were observed, the band associated with the tetramer showed a diffuse extension towards the anode.

When the enzyme was pre-incubated with either EPSP or FMN, similar results were observed. If either of these ligands remained bound during the 45 min period of the experiment, they clearly did not affect the mobility of the protein through the gel. More probably, if these anionic ligands did not bind tightly, they would have become electrophoretically separated from the protein during the experiment, and any potential change of mobility would not have been apparent with this system. This is certainly the case with oxidized FMN alone, because a half-life of approx. 30 s for the binary complex (calculated from the dissociation rate constant determined above) is clearly short compared with the 45 min duration of the electrophoresis experiment.

By contrast, when the enzyme was pre-incubated with both EPSP and oxidized FMN, none of the protein migrated to the same position. Instead, the protein migrated further towards the anode in a broad band spanning apparent molecular masses of about 140 and 150 kDa, which are a little closer to that predicted. Although the protein band was broader, it was more defined in that it did not show any sign of the diffuse extension towards the anode. Again, no monomers, dimers or higher oligomers were observed. Similar results were observed when the enzyme was pre-incubated with FMN and the substrate analogue (6*R*)-6-fluoro-EPSP (results not shown).

Effects of EPSP and oxidized FMN on the susceptibility of chorismate synthase to tryptic digestion

Firm evidence that the binding of EPSP and oxidized FMN affects the structure of chorismate synthase was obtained from tryptic digests of the protein in the absence and presence of EPSP and oxidized FMN, as is shown in Figure 5. In the absence of EPSP and FMN (lane 5), or in the presence of only one of the two (lanes 3 and 4), chorismate synthase was readily digested by trypsin. In the presence of both EPSP and oxidized FMN, however, chorismate synthase was remarkably stable towards the proteolytic activity of trypsin over a period of 1 h at 25 °C (lane 2). The presence of either EPSP alone or FMN alone did not afford even partial protection.

Effects of EPSP and oxidized FMN on the far-UV CD spectrum of chorismate synthase

The CD spectrum of chorismate synthase is shown in Figure 6. The presence of either EPSP alone or both EPSP and oxidized FMN, whereby over 95% of the protein is expected to form the ternary complex, had only minor effects on the CD spectrum. A secondary structure prediction based on the CD spectrum of chorismate synthase alone (Figure 6, solid line) was obtained using the program SELCON [27]. From two independent measurements, the calculation yielded a distribution of: α-helix, $30.4 \pm 1\%$; β-sheet, $21.8 \pm 0.5\%$; loops, $27.4 \pm 0.2\%$; others, $19.5 \pm 0.1\%$.

Effects of EPSP and oxidized FMN on the FT-IR spectrum of chorismate synthase

The second derivative spectrum of unliganded chorismate synthase is shown in Figure 7(A). The observed peaks can be assigned to the secondary structure elements as follows [35]: 1691.5 cm^{-1} and 1665 cm^{-1}, turns; 1656 cm^{-1}, α-helix; 1635.5 cm^{-1}, β-strands for the amide I region; and 1548.5 cm^{-1}, α-helix; 1518.5 cm^{-1}, β-strand for the amide II region. Thus the presence of both α-helix and β-sheet is confirmed by this technique. In the ternary complex with EPSP and oxidized FMN (Figure 7B), although the peaks at 1691.5 cm^{-1} (turns), 1634.5 cm^{-1} (β-strands), 1549.5 cm^{-1} (amide II, α-helix) and 1518 cm^{-1} (amide II, β-strand) remained at similar positions, the signals at 1665 cm^{-1} (turns) and 1656 cm^{-1} (α-helix) appeared to be slightly shifted to higher wavenumbers. In addition, new peaks were observed at 1650 cm^{-1}, 1620 cm^{-1} and 1581 cm^{-1}, as

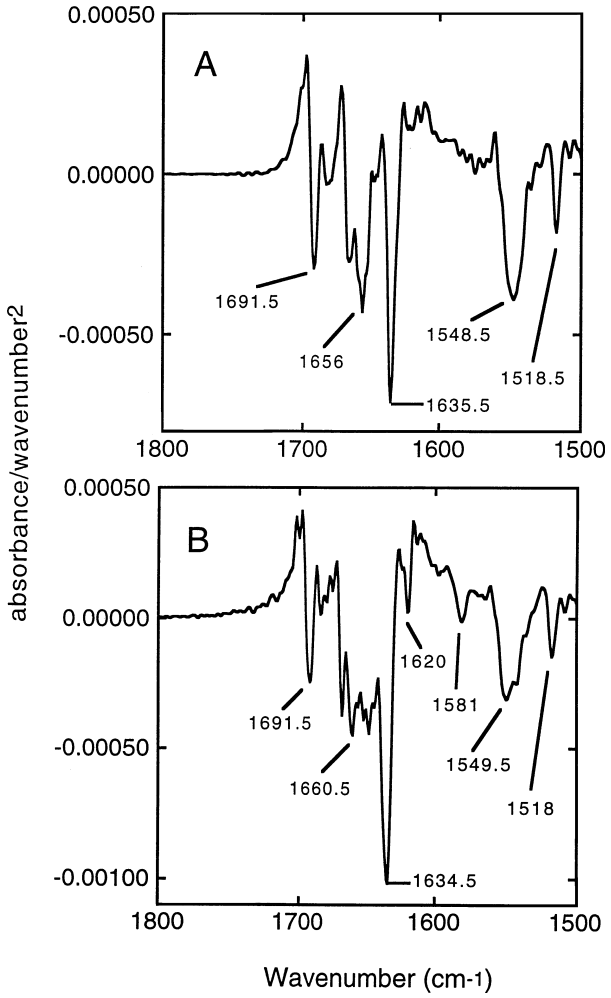

Figure 7 Changes in the FT-IR spectrum of chorismate synthase on addition of both EPSP and oxidized FMN

Second-derivative spectra are shown of the deconvoluted FT-IR spectra of chorismate synthase (0.5 mM) in the absence (**A**) and presence (**B**) of both EPSP and FMN in 10 mM potassium phosphate buffer, pH 7.5, at 25 °C. See the Results section for the peak assignments and a description of the differences between the two spectra.

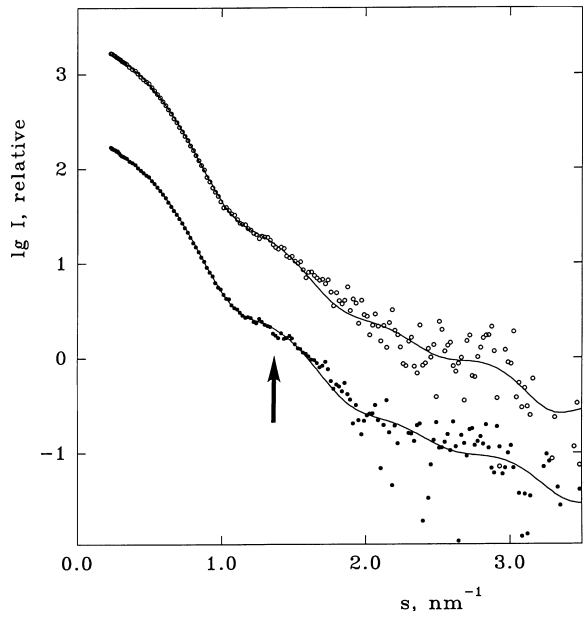

Figure 8 Changes in the small-angle X-ray scattering data of chorismate synthase with and without both EPSP and oxidized FMN

Experimental scattering data (○, ●) from chorismate synthase in 100 mM sodium potassium phosphate buffer, pH 6.9, at 22 °C are shown along with the curves calculated from the restored shapes in Figure 9 (solid lines). ○, Chorismate synthase (0.18 mM); ●, chorismate synthase with EPSP and FMN (0.2 mM each). The ● points and their fitted curve are displaced one logarithmic unit down for clarity. The first subsidiary maximum is indicated by the arrow. See the Results section for a description of the quantitative and qualitative differences between the two data sets.

well as other minor changes. With free FMN, peaks at 1582 cm^{-1} and 1549 cm^{-1} were observed, and free EPSP showed no peak in the spectral range of interest. Therefore the peaks at 1581 cm^{-1} and the shoulder at 1548 cm^{-1} can be assigned to the FMN moiety. The two remaining new peaks at 1650 cm^{-1} and 1620 cm^{-1} must be attributed to the protein, and are best interpreted as changes in the α-helical and β-strand structural elements of chorismate synthase. Hence formation of the ternary complex of chorismate synthase, EPSP and oxidized FMN appears to generate structural changes in α-helical as well as β-strand secondary-structural elements.

Effects of EPSP and oxidized FMN on small-angle X-ray scattering by chorismate synthase

Solution scattering curves of native chorismate synthase apoenzyme and the ternary complex with EPSP and FMN are presented in Figure 8. Comparison of the normalized forward scattering with the values obtained with a reference solution of BSA yields a molecular mass of 150 kDa for both forms. This result is in agreement with the estimates from the native gel electrophoresis described above and with earlier reports that chorismate synthase exists as a homotetramer in solution [7]. The maximum size of unliganded chorismate synthase was found to be $D_{max} = 11 \pm 0.5$ nm and its radius of gyration was $R_g = 3.37 \pm 0.02$ nm; the parameters of the ternary complex were $D_{max} = 10.5 \pm 0.5$ nm and $R_g = 3.28 \pm 0.02$ nm. Furthermore, as seen from the visual comparison of the two experimental data sets in Figure 8, the first subsidiary maximum in the curve from liganded chorismate synthase (indicated by an arrow) is more pronounced than that for unliganded enzyme. This, together with the changes in R_g and D_{max}, indicates that the enzyme has a somewhat more compact overall shape upon formation of the ternary complex with EPSP and oxidized FMN.

This qualitative conclusion is further supported by the results of the *ab initio* shape determination. The particle envelopes restored, as described in the Experimental section at a resolution of 2 nm, are presented in Figure 9, and the fits to the experimental data are shown in Figure 8. The portions of the scattering curves up to $s_{max} = 3.5$ nm^{-1} were used in the shape determination, and the final *R*-factors of the restored shapes were 1.0 % and 1.1 % for unliganded and liganded chorismate synthase respectively. Comparison of the two envelopes indicates that the compaction of liganded chorismate synthase is achieved by 'correlated screw movements' of the particle domains which can be identified as monomers. To verify the significance of the observed differences, several shape restorations were performed under different minimization conditions, in particular those where the model of one form was used as an initial approximation to restore the shape of the other; in all cases, shapes very similar to those in Figure 9

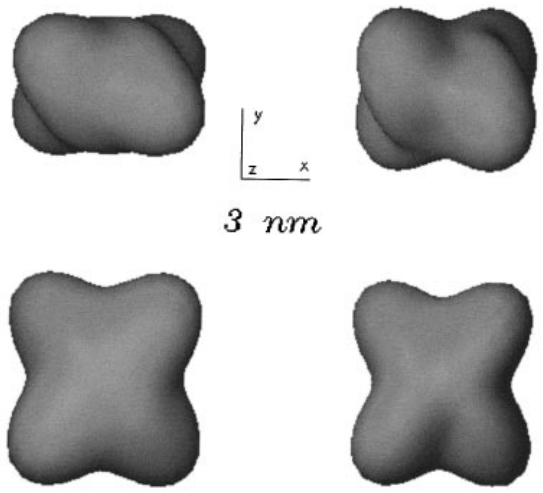

Figure 9 Changes in the envelopes of chorismate synthase in the presence of both EPSP and oxidized FMN

Low-resolution envelopes of chorismate synthase alone (upper and lower left) are compared with those of the ternary complex of chorismate synthase with EPSP and FMN (upper and lower right) restored from the scattering data (Figure 8). The binding of EPSP and FMN clearly results in correlated screw movements within the homotetrameric enzyme. The lower shapes are 90° anticlockwise rotations along the *x*-axis of the upper shapes.

were obtained. The uniqueness of the shape restoration is also supported by the analysis of the information content in the experimental data. As shown by Svergun et al. [21], low-resolution shape determination is unique when the number of independent parameters in the model (M) does not exceed 1.5 times the number of Shannon channels (N_s) in the experimental data, where $N_s = D_{max}s_{max}/\pi$. In our case, $N_s = 12$, and thus the value $M = 13$ (see the Experimental section) is well within this limit. Considering the envelopes in Figure 9, one should bear in mind that they were obtained assuming a 222-point symmetry, which allowed a significant decrease in the number of free parameters in the model. Without symmetry, description of a particle envelope up to $L = 6$ would require 43 independent parameters. The models should therefore be considered unique only within the symmetry restriction, although assuming a 222 symmetry is justified for a homotetramer. A similar low-resolution model obtained from the solution scattering data for tetrameric yeast pyruvate decarboxylase [36,37] was later confirmed by protein crystallography [38].

Secondary and tertiary structure prediction based on the amino acid sequence of *E. coli* chorismate synthase

Since the type-1 discrete state-space modelling [28,29] is restricted to a sequence length of up to 350 amino acids, the amino acid sequence of *E. coli* chorismate synthase was trimmed by the N-terminal methionine and the last 10 amino acids of the C-terminus. The C-terminal fragment does not contain any conserved amino acids according to sequence alignments of all known chorismate synthase sequences (see the Experimental section). More importantly, Charles et al. [39] demonstrated that the deletion of the C-terminal 36 amino acids did not affect the correct folding and catalytic activity of the enzyme. In any case, similar modelling results were obtained when the first 11 N-terminal amino acids were omitted.

The sequence analysis shows that *E. coli* chorismate synthase has a probability of 1.0 of belonging to the super-class of α–β

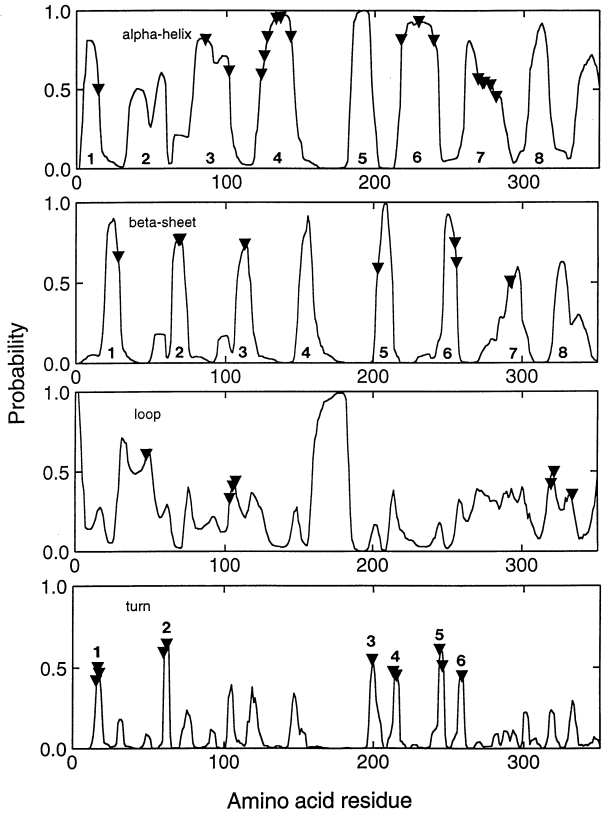

Figure 10 Secondary structure prediction for *E. coli* chorismate synthase and strictly conserved amino acids

The four graphs show the probability of an amino acid residue to be in (from top to bottom) an α-helix, a β-strand, a loop or a turn, according to type-1 discrete state-space modelling. A total of eight repeating α/β units are predicted with high probability, which are consistent with an α–β-barrel. Residues labelled with inverted triangles mark strictly conserved amino acids among the 18 chorismate synthases listed in the Experimental section (17 in α-helices, 11 in turns, eight in β-strands and seven in loops). Note that the N-terminal methionine and the ten C-terminal amino acids were omitted from the analysis, and the remaining sequence is numbered from 1 to 350 accordingly.

proteins. Within this family of proteins, the program predicted a probability of 1.0 that the sequence folds into an α–β-barrel (ab8bl) tertiary structure. It predicted nine α-helices, eight β-strands, one extended loop in the middle of the sequence and six turns with a probability of at least 0.5, as shown in Figure 10. Using a minimal probability of 0.5 as a classifying criterion, the distribution of secondary structures was: α-helix, 44.0%; β-strands, 20.6%; loops, 18.6%; turns, 2.6%; 14.2%, unassigned.

A total of 17 out of 43 strictly conserved amino acid residues are located in α-helices, predominantly in helices 4 and 7 (Figure 10). The first of these two clusters of conserved amino acid residues (Arg-102, Pro-103, His-105, Asp-107, Lys-113, Arg-124, Ser-126, Arg-128, Val-134 and Gly-137; the numbering is taken from the *E. coli* sequence without the N-terminal methionine) is rich in charged and polar amino acid residues, whereas the cluster in helix 7 is composed of uncharged amino acid residues (Asn-270, Gly-273, Gly-274, Gly-278 and Gly-282). A total of 11 amino acid residues are conserved in the six areas predicted to be turns or, in other words, 50% of all amino acid residues in this structural element are strictly conserved among chorismate synthases. Conserved amino acid residues are found in neither the extended loop region nor the preceding β-sheet or following α-helix. This region also varies significantly in length and sequence among chorismate synthases from different species.

DISCUSSION

In this paper, we present a number of spectroscopic and physical studies which show that chorismate synthase undergoes a major structural change when both oxidized FMN and EPSP are bound. The small-angle X-ray scattering data indicate that the enzyme has a more compact overall shape in the ternary complex. The correlated screw movements are immediately apparent when the shapes are determined from the data. This difference in shape between the two enzyme states is considered to be significant, because very similar models are obtained when the model from one form is used as an initial approximation in the determination of the other. In addition, these experiments show that there is no change in the oligomerization state of the tetrameric enzyme.

The protection from tryptic digestion of the protein in the ternary complex provides additional strong evidence for a structural change. Neither EPSP alone nor FMN alone afforded any such protection. This result is consistent with the decreased reactivity of free cysteine residues with 5,5′-dithiobis-(2-nitrobenzoic acid) on forming the ternary complex [40]. Such a significant structural change could result in changes in the distribution and environment of secondary-structural elements within the protein. A lack of significant changes in the far-UV CD spectrum of the protein indicates that the overall relative proportions of secondary-structural elements do not change significantly. However, changes in the FT-IR spectrum strongly suggest that changes in the environment of both α-helical and β-strand elements do indeed occur.

The ternary complex exhibits increased mobility during non-denaturing PAGE. None of the complex migrated to the same position as the majority of the apoprotein. Since it was subjected to PAGE for a period of 45 min, the complex must be very stable to dissociation, having a half-life at least of the order of tens of minutes. Rather than the increase in mobility being the result of a decrease in hydrodynamic volume, consistent with the small-angle scattering data, it could be due simply to an increase in overall negative charge on binding of the substrate and cofactor. Attempts to address this by using two-dimensional isoelectric focusing PAGE were hampered by precipitation of the apoenzyme in the gels. Theoretically, the pI of the ternary complex could become more negative by up to 0.5 unit and, at the pH of 8.8 used in the non-denaturing PAGE experiment, the complex could have up to six additional net negative charges. However, the enzyme alone migrated as a diffuse band which extended towards and beyond the position to which the ternary complex migrated. This is difficult to explain in terms of a distribution of differently charged species. It is much more easily explained by a distribution of species with different hydrodynamic volumes, with the majority species having the larger hydrodynamic volume. In other words, these experiments indicate that the apoprotein exhibits a degree of flexibility that the ternary complex does not.

Alterations in the visible CD spectrum of the enzyme-bound FMN on binding of EPSP show that the environment of the flavin changes considerably. Comparisons of spectral alterations with those of other flavoproteins [41–44] for which X-ray crystal structures are known [45,46] indicate that such alterations are not easily rationalized in terms of specific structural changes. In addition, alterations in spectra can occur on binding of substrates adjacent to the flavin, in the absence of any major change in the structure of the protein. However, we cannot rule out the possibility that the alterations observed with chorismate synthase reflect, at least in part, changes in protein structure.

Encouraged by the successful prediction of the tertiary structure of flavodoxin using discrete state-space modelling [28], we have used this method to obtain the first *bona fide* prediction for the secondary and tertiary structure of chorismate synthase. The results of this method are consistent with those obtained by CD and FT-IR spectroscopy, in that chorismate synthase is composed of both of α-helix and β-strands. The percentages of β-strands are in good agreement, but the model predicted a higher α-helical content. The modelling predicted that chorismate synthase has an α–β-barrel fold with a probability of 1.0, and ruled out 15 other possible model structures. Half of all the amino acids predicted to be in turns are strictly conserved among chorismate synthases. Since turns are important structural constraints of a protein structure, this result increases our confidence in the predicted structure. Additional confidence comes from the X-ray crystal structure of the allosteric enzyme pyruvate kinase type I, which shares sequence similarity with the chorismate synthases and has an α–β-barrel at its core [47]. Although the sequence similarity between the two enzymes is significant, it is not sufficient to allow homology modelling.

The bifunctional chorismate synthases from the fungi *Neurospora crassa* and *Saccharomyces cerevisiae* have an additional NADPH:FMN oxidoreductase activity. The NADPH-binding site has been postulated to involve amino acid residues [48] that map to helix 6, turn 5, strand 6 and turn 6 (see Figure 10). A number of conserved amino acid residues are located in this region. It remains to be seen whether this region forms the structural scaffold for the oxidoreductase activity in fungal chorismate synthases. The cluster of conserved amino acids in helix 7 is rich in uncharged small amino acid residues (mainly glycine). By contrast, the cluster in helix 4 includes one acidic and five basic amino acids. It appears likely that this cluster of amino acids in helix 4 could be involved in the binding of the FMN cofactor and of EPSP, and in catalysis. This hypothesis is currently being tested by site-directed mutagenesis experiments using *E. coli* chorismate synthase.

In summary, we can conclude that chorismate synthase undergoes a major change in protein structure on binding oxidized FMN and EPSP. In addition, electrophoresis experiments indicate that the apoenzyme probably exhibits more conformational flexibility than the ternary complex. The enzyme can bind either oxidized FMN alone, leading to the quenching of tryptophan fluorescence, or EPSP alone, leading to an increase in protein solubility and a delay in FMN binding. However, it is clear that the ternary complex forms only when oxidized FMN binds before EPSP. Furthermore, the increase in the affinity of the enzyme for oxidized FMN and the lowering of the FMN redox potential by EPSP show that their binding sites are not independent [9]. The complete lack of protection by either EPSP alone or FMN alone to tryptic digestion shows that the structural change requires the binding of both. It is not clear whether this tetrameric enzyme exhibits co-operative binding, as no study to date has revealed any. Nevertheless, the stable ternary complex between enzyme, EPSP and oxidized FMN can be considered to be a good structural model of the corresponding active ternary complex formed with reduced FMN immediately before catalysis commences. A similar study using the cofactor and substrate analogues 5-deaza-$FMNH_2$ [49,50] and (6*R*)-6-fluoro-EPSP [51], which also preclude normal turnover, would shed more light on the structural change. In the absence of a high-resolution structure of the enzyme, it is not possible to define the nature of the structural changes. However, they are significant changes which are likely to be important during the catalytic cycle of chorismate synthase.

P. M. thanks the E. C. for an E. C. Senior Scientist fellowship under the Human Capital and Mobility Programme (contract # ERBCHBICT941301). S. B. thanks the BBSRC/MRC/DTI Protein Engineering Link Programme, Zeneca Pharmaceuticals and

Zeneca Agrochemicals for their support. We thank Dr. S. George for his initial help with the FT-IR spectroscopy, and Dr. J. Oelichmann and Dr. A. Rau (Perkin–Elmer Werk, Überlingen, Germany) for their generous support during the course of the FT-IR measurements.

REFERENCES

1 Roberts, F., Roberts, C. W., Johnson, J. J., Kyle, D. E., Krell, T., Coggins, J. R., Coombs, G. H., Milhous, W. K., Tzipori, S., Ferguson, D. J. P. et al. (1998) Nature (London) **393**, 801–805
2 Hill, R. K. and Newkome, G. R. (1969) J. Am. Chem. Soc. **91**, 5893–5894
3 Floss, H. G., Onderka, D. K. and Carroll, M. (1972) J. Biol. Chem. **247**, 736–744
4 Onderka, D. K. and Floss, H. G. (1969) J. Am. Chem. Soc. **91**, 5894–5896
5 Morell, H., Clark, M. J., Knowles, P. F. and Sprinson, D. B. (1967) J. Biol. Chem. **242**, 82–90
6 Welch, G. R., Cole, K. W. and Gaertner, F. H. (1974) Arch. Biochem. Biophys. **165**, 505–518
7 White, P. J., Millar, G. and Coggins, J. R. (1988) Biochem. J. **251**, 313–322
8 Bornemann, S., Ramjee, M. K., Balasubramanian, S., Abell, C., Coggins, J. R., Lowe, D. J. and Thorneley, R. N. F. (1995) J. Biol. Chem. **270**, 22811–22815
9 Macheroux, P., Petersen, J., Bornemann, S., Lowe, D. J. and Thorneley, R. N. F. (1996) Biochemistry **35**, 1643–1652
10 Macheroux, P., Bornemann, S., Ghisla, S. and Thorneley, R. N. F. (1996) J. Biol. Chem. **271**, 25850–25858
11 Macheroux, P., Bornemann, S. and Thorneley, R. N. F. (1997) in Flavins and Flavoproteins 1996 (Stevenson, K. J., Massey, V. and Williams, C. H. J., eds.), pp. 113–122, University of Calgary Press, Calgary, Canada
12 Bornemann, S., Lowe, D. J. and Thorneley, R. N. F. (1996) Biochemistry **35**, 9907–9916
13 Bornemann, S., Balasubramanian, S., Coggins, J. R., Abell, C., Lowe, D. J. and Thorneley, R. N. F. (1995) Biochem. J. **305**, 707–710
14 Knowles, P. F., Levin, J. G. and Sprinson, D. B. (1970) Methods Enzymol. **17**, 360–362
15 Laemmli, U.K. (1970) Nature (London) **227**, 680–685
16 Boulin, C., Kempf, R., Koch, M. H. J. and McLaughlin, S. M. (1986) Nucl. Instrum. Methods Phys. Res. Sect. A **A249**, 399–407
17 Boulin, C. J., Kempf, R., Gabriel, A. and Koch, M. H. J. (1988) Nucl. Instrum. Methods Phys. Res. Sect. A **A269**, 312–320
18 Koch, M. H. J. and Bordas, J. (1983) Nucl. Instrum. Methods **208**, 461–469
19 Gabriel, A. and Dauvergne, F. (1982) Nucl. Instrum. Methods **201**, 223–224
20 Svergun, D. I. (1993) J. Appl. Crystallogr. **26**, 258–267
21 Svergun, D. I., Semenyuk, A. V. and Feigin, L. A. (1988) Acta Crystallogr. **A44**, 244–250
22 Svergun, D. I. (1992) J. Appl. Crystallogr. **25**, 495–503
23 Svergun, D. I. and Stuhrmann, H. B. (1991) Acta Crystallogr. **A47**, 736–744
24 Svergun, D. I., Volkov, V. V., Kozin, M. B. and Stuhrmann, H. B. (1996) Acta Crystallogr. **A52**, 419–426
25 Svergun, D. I. (1997) J. Appl. Crystallogr. **30**, 792–797
26 Feigin, L. A. and Svergun, D. I. (1987) Structure Analysis by Small-Angle X-Ray and Neutron Scattering, Plenum Press, New York
27 Sreerama, N. and Woody, R. W. (1993) Anal. Biochem. **209**, 32–44
28 Stultz, C. M., White, J. V. and Smith, T. F. (1993) Protein Sci. **2**, 305–314
29 White, J. V., Stultz, C. M. and Smith, T. F. (1994) Math. Biosci. **119**, 35–75
30 Klenk, H. P., Clayton, R. A., Tomb, J. F., White, O., Nelson, K. E., Ketchum, K. A., Dodson, R. J., Gwinn, M., Hickey, E. K., Peterson, J. D. et al. (1997) Nature (London) **390**, 364–370
31 Tomb, J. F., White, O., Kerlavage, A. R., Clayton, R. A., Sutton, G. G., Fleischmann, R. D., Ketchum, K. A., Klenk, H. P., Gill, S., Dougherty, B. A. et al. (1997) Nature (London) **388**, 539–547
32 Bult, C. J., White, O., Olsen, G. J., Zhou, L. X., Fleischmann, R. D., Sutton, G. G., Blake, J. A., Fitzgerald, L. M., Clayton, R. A., Gocayne, J. D. et al. (1996) Science **273**, 1058–1073
33 Ramjee, M. K. (1992) Ph.D. Thesis, University of Sussex, Brighton, U.K.
34 Ramjee, M. K., Coggins, J. R., Hawkes, T. R., Lowe, D. J. and Thorneley, R. N. F. (1993) Bioorg. Med. Chem. Lett. **3**, 1409–1414
35 Wantyghem, J., Baron, M. H., Picquart, M. and Lavialle, F. (1990) Biochemistry **29**, 6600–6609
36 Konig, S., Svergun, D. I., Koch, M. H. J., Hubner, G. and Schellenberger, A. (1992) Biochemistry **31**, 8726–8731
37 Konig, S., Svergun, D. I., Koch, M. H. J., Hubner, G. and Schellenberger, A. (1993) Eur. Biophys. J. **22**, 185–194
38 Dyda, F., Furey, W., Swaminathan, S., Sax, M., Farrenkopf, B. and Jordan, F. (1993) Biochemistry **32**, 6165–6170
39 Charles, I. G., Lamb, H. K., Pickard, D., Dougan, G. and Hawkins, A. R. (1990) J. Gen. Microbiol. **136**, 353–358
40 Bornemann, S., Lowe, D. J. and Thorneley, R. N. F. (1996) Biochem. Soc. Trans. **24**, 84–88
41 Edmondson, D. E. and Tollin, G. (1971) Biochemistry **10**, 124–132
42 Edmondson, D. E. and Tollin, G. (1971) Biochemistry **10**, 113–124
43 Tollin, G. (1968) Biochemistry **7**, 1720–1727
44 Hesp, B., Calvin, M. and Hosokawa, K. (1969) J. Biol. Chem. **244**, 5644–5655
45 Burnett, R. M., Darling, G. D., Kendall, D. S., LeQuesne, M. E., Mayhew, S. G., Smith, W. W. and Ludwig, M. L. (1974) J. Biol. Chem. **249**, 4383–4392
46 Wierenga, R. K., De Jong, R. J., Kalk, K. H., Hol, W. G. J. and Drenth, J. (1979) J. Mol. Biol. **131**, 55–73
47 Mattevi, A., Valentini, G., Rizzi, M., Speranza, M. L., Bolognesi, M. and Coda, A. (1995) Structure **3**, 729–741
48 Henstrand, J. M., Amrhein, N. and Schmid, J. (1995) J. Biol. Chem. **270**, 20447–20452
49 Lauhon, C. T. and Bartlett, P. A. (1994) Biochemistry **33**, 14100–14108
50 Bornemann, S., Coggins, J. R., Lowe, D. J. and Thorneley, R. N. F. (1995) in Perspectives on Protein Engineering and Complementary Technologies 1995 (Geisow, M. J. and Epton, R., eds.), pp. 134–135, Mayflower Worldwide Ltd., Birmingham, U.K.
51 Ramjee, M. N., Balasubramanian, S., Abell, C., Coggins, J. R., Davies, G. M., Hawkes, T. R., Lowe, D. J. and Thorneley, R. N. F. (1992) J. Am. Chem. Soc. **114**, 3151–3153

Received 18 June 1998/22 July 1998; accepted 13 August 1998